Hindawi
Mathematical Problems in Engineering
Volume 2020, Article ID 9267838, 13 pages
https://doi.org/10.1155/2020/9267838

Research Article

Modeling and Optimization for Fault Diagnosis of Electromechanical Systems Based on Zero Crossing Algorithm

Qing Chen,[1] **Tao Liu**,[1] **Xing Wu**,[1,2] **and Hua Li**[1]

[1]*Key Laboratory for Advanced Equipment Intelligent Manufacturing Technology of Yunnan Province, Kunming University of Science and Technology, Kunming 650500, China*
[2]*Yunnan Vocational College of Mechanical and Electrical Technology, Kunming 650203, China*

Correspondence should be addressed to Tao Liu; kmliutao@aliyun.com

Received 24 April 2020; Accepted 30 June 2020; Published 27 July 2020

Guest Editor: Jian Huang

The demand of system security and reliability in the modern industrial process is ever-increasing, and fault diagnosis technology has always been a crucial research direction in the control field. Due to the complexity, nonlinearity, and coupling of multitudinous control systems, precise system modeling for fault diagnosis is attracting more attention. In this paper, we propose an improved method of electromechanical systems fault diagnosis based on zero-crossing (ZC) algorithm, which can present the calculation model of zero-crossing rate (ZCR) and optimize the parameters of ZC algorithm by establishing a criterion function model to improve the diagnosis accuracy and robustness of ZC characteristic model. The simulation validates the influence of different signal-to-noise ratio (SNR) on ZC feature recognition ability and indicates that the within-between distance model is effective to enhance the diagnose accuracy of ZC feature. Finally, the method is applied to the diagnosis of motor fault bearing, which confirms the necessity and effectiveness of the model improvement and parameter optimization and verifies the robustness to the load.

1. Introduction

The electromechanical system is a vital part in the process of modern industrial production and manufacturing. The research of fault diagnosis and prediction methods, which can be applied to nonlinear electromechanical systems and realize the real-time monitoring, diagnosis, prediction, and state-based maintenance of electromechanical system, has an important significance for improving the safety and reliability of electromechanical system. As a crucial component of electromechanical systems, the stability and reliability of motor operation directly affect the normal operation of electromechanical systems, especially in the fields of CNC machine tools [1], robots [2], and aircraft [3], which require relatively high production accuracy, efficiency, and reliability. In particular, rolling element bearings (REBs) are the most commonly machine elements used in almost all rotary machinery and is also the vulnerable component of rotating machinery [4, 5]. The health status of REBs directly affects the functioning of the motor, which accounts for almost 40–50% of motor fault [6, 7]. As a consequence, the fault diagnosis of motor REBs plays a crucial role to the smooth, reliable, and safe handling of the whole electromechanical system.

Mathematical modeling and analysis are useful to design and study control systems [8–10] and also can be used to analyze the behavior of the real systems under different operating conditions, test signal processing methods, and new detection and prognosis techniques. Over the last few decades, the dynamic modeling of rolling bearings has been extensively studied. McFadden and Smith established a model to illustrate the vibration characteristics of a single point defect in the inner race of REB under the same radial load. The model comprehensively considers the impacts of bearing geometry, bearing size distribution, transfer function, and vibration index attenuation. By comparing the radial vibration spectra predicted with measured, the excellent performance of the model is validated [11]. Sawalhi

and Randall proposed a combination of gear and bearing dynamic model. In this model, the outspread faults of the inner and outer rings of REBs in the presence of gear interactions can be studied [12]. Due to the distinct superiority of U-model in nonlinear control, the development of U-model based gear and bearing state prediction is promising [13, 14]. For the sake of research of the nonlinear dynamic characteristics of the REB system containing surface defect, a theoretical model is presented by Rafsanjani et al. In order to investigate the linear stability of the defective bearing rotor system with changes in the parameters of the conversion system, the classic Floquet theorem was embedded in this model. In the solution of this model, the peak-to-peak frequency response of the system was obtained in some cases, and the basic paths of offset, collimation, and chaotic motion for different internal radial clearance were determined [15]. Based on the research of the dynamic model on REB, the fault diagnosis using the measurement signal in the system has been developed rapidly. In the process of system operation, the symptoms of failure will be reflected in the detection information (measurement signal), the resultful features of the signal will be extracted by means of analysis, and then the diagnosis scheme will be established based upon the fault symptom analysis and the prior knowledge of the healthy system. Nevertheless, the quality of features extracted from signals is always a thorny problem. Since the vibration data of a faulty rolling bearing is usually unstable and nonlinear and contains relatively weak fault features, it has always attracted wide attention from researchers. Over the past decades, a mass of approaches of feature extraction for REB fault diagnosing have been proposed, which can be roughly summarized as the following categories according to the distinction of principles and properties. Firstly, feature extraction based on the traditional time domain parameters, for example, crest factor, peak-to-peak value, kurtosis, root-mean square, shape factor, and standard deviation etc. [16–18]; secondly, frequency domain parameters, such as power spectral density, power spectrum [19]; thirdly, analysis based on time-frequency domain methods, for instance, spectrogram and wavelet transform [20–22]; finally, based on multiple parameters the mixed feature extraction realized, for example, the method of [23, 24] have extracted blended parameter features of time domain, frequency domain, and time-frequency.

It is found that in most former feature extraction techniques, a large number of complex calculations are needed for vibration signal data for improving the accuracy of fault identification. Compared with these traditional methods, as ZC features generate directly from the count of the ZC interval in the time domain, ZC feature algorithm has an obvious advantage, which can well reflect the change of signal frequency with fast convergence, and is easy to calculate. Therefore, ZC algorithm has been successfully applied to speech recognition [25], vehicle classification [26], and biomedical applications [27, 28]. Moreover, the ZC method is also commonly used in signal processing and mechanical fault diagnosis. William and Hoffman showed the ZC method combined with an ANN is effective in early detection and diagnosis of bearing failures [29]. Liu et al. proposed a bearing performance degradation estimation method based on the ZC characteristics and coupled hidden Markov model and proved that the ZC features can detect the early degradation stage of the bearing [30]. Ukil et al. presented a feature extraction method of current ZC moment to detect short-circuit fault of stator winding of series asynchronous induction motors [31]. Gonzalez and Kinsner showed that ZC could be used to identify different parts of the composite signal, and the advantage of the ZC computing immediately in the time domain is attractive to real time implementation [32]. Waghmare et al. presented a methodology based on piecewise energy and corresponding mean of signal ZC in environmental noise, which has a broad application prospect in dealing with the underwater target-radiated noise [33]. For the first time, Nayana and Geethanjali used time domain parameters, waveform parameters, slope sign changes (SSC), simple sign integral, and Wilson amplitude to established mean absolute value and ZC to identify failures of motors, and by comparing with conventional features, they proved the proposed features perform better [34].

Literatures [29, 30] demonstrated the advantages of ZC features in bearing fault diagnosis, such as small computation and fast speed. However, by reason of no stationary and nonlinearity of REB fault signals, the recognition rate of the extracted ZC features in REB fault recognition is low, especially in the case of low signal-to-noise ratio (SNR). For solving this problem, this paper firstly analyzes the recognition ability of ZC features under different SNR conditions, then proposes an adaptive method to enhance the capable of recognition fault, and verifies the recognition rate through neural network. The improved fault diagnosis method for electromechanical system which optimized the calculation model of ZCR and optimized the parameters of ZC algorithm by establishing a criterion function model greatly improves the fault recognition rate and is robust to the load.

The remaining of this article is organized as follows. In Section 2, the theory of ZC feature algorithm is briefly reviewed and the improved model of ZC calculation and the method of parameters optimized through modeling a criterion function with within-between distance are introduced, and Section 3 simulation signals are used to verify the influence of ZC feature recognition ability at disparate SNR and verifies the validation of the presented method. In Section 4, the experiment is analyzed to verify the method, and the conclusions are given in the Section 5.

2. Theoretical Background

2.1. ZC Characteristic Feature Algorithm. The measures widely used to represent the characteristics of ZC include the mean ZCR, density of the time interval between continuous ZCs, and excess threshold measure. According to the experience of literature [33], compared with other ZC measurements, the ZC feature of excess threshold measurement is more conducive to fault diagnosis at relatively high SNR. Therefore, in this paper, the ZC feature of excess threshold measurement is used to method improvement and

parameter optimization for achieving the more accuracy of fault diagnosis at low SNR.

In order to describe the short-time waveform, the time domain signal collected should be divided into a diminutive observation window, firstly. In addition, the measure of the observation window should be greater than the maximum expected duration between continuous ZCs. T_L is defined as the measure of the observation window, T_Q represents the maximum expected duration between the continuous ZCs, and $T_Q \le T_L$. Then, divide the duration range $[0, T_Q]$ into Q intervals by the threshold of $Q+1$, and define T_i as the ith interval. Let C_i represent the count of ZC intervals with duration in the range of T_{j-1} and T_j and $x(n)$ is the short-time waveform with the data sequence N, then C_i can be obtained by

$$C_i = \frac{1}{2}\sum_{n=2}^{N}[\operatorname{sgn}[x(n)] - \operatorname{sgn}[x(n-1)]], \tag{1}$$

where the $\operatorname{sgn}[x]$ is sign function and expressed as

$$\operatorname{sgn}[x(n)] = \begin{cases} 1\,(x \ge 0), \\ -1\,(x < 0). \end{cases} \tag{2}$$

Then, the eigenvector of ZC counts is normalized by the observation window, and defined as

$$F_{\text{count}} = \frac{C}{T_L} = \frac{1}{T_L}\left(C_1 C_2 \dots C_Q\right), \tag{3}$$

and the function of excess threshold measurement can be calculated by the following formula:

$$f(T_i) = \frac{1}{2}\sum_{k=j}^{Q-1} C_{k+1}\left(T_k + T_{k+1}\right), \tag{4}$$

where $1/2C_{k+1}(T_k + T_{k+1})$ is used to approximately calculate the sum of ZC durations in the range $T_k < T \ll T_{k+1}$.

Thereby, the eigenvector of excess threshold measurement can be obtained by

$$F_{\text{duration}} = \frac{1}{T_L}\left[f(T_0), f(T_0), \dots, f\left(T_{Q-1}\right)\right]. \tag{5}$$

2.2. Criterion Function Modeling. The purpose of feature extraction is to acquire the most available information related to the equipment condition so as to realize fault identification. The classification ability of feature vectors directly determines the ability of fault recognition. Based on the idea of Fisher criterion [35] to calculate the distance between categories and within categories, the recognition ability of features can be improved by finding a functional relationship between the intraclass distance and interclass distance of features. In other words, the smaller the intraclass distance and the larger the interclass distance of the feature clustering results, the higher the discrimination degree of the classification results will be. Therefore, we can construct a criterion function that reflects the within-between distance.

Assume that the feature set $(x_1, x_2, \dots, x_N)$ to be classified is classified as class $C\{x_i^{(j)}, \quad j = 1, 2, \dots C; i = 1, 2, \dots n_j\}$. The data quantity of class j is n_j. The intraclass distance of class j can be expressed as follows:

$$S_w^{(j)} = \frac{1}{n_j}\sum_{i=1}^{n_j}\left(x_i^{(j)} - m_j\right)\left(x_i^{(j)} - m_j\right)^T, \tag{6}$$

where m_j is the average of the samples of class j and $m_j = 1/n_j \sum_{i=1}^{n_j} x_i^{(j)}$, $(j = 1, 2, \dots, C)$.

Let $S_w^{(k)}$ and m_k denote the intraclass distance and the samples mean of class k ($k \ne j$ and $k \le C$), respectively, the interclass distance between class j and k can be expressed as follows:

$$S_B = \sum\left(m_j - m_k\right)\left(m_j - m_k\right)^T. \tag{7}$$

Then, the function represents the ability to recognize between classes can be expressed as follows:

$$I = \frac{S_B}{S_w^{(j)} + S_w^{(k)}}. \tag{8}$$

On the premise that the highest recognition capacity of the two categories is not weakened, let us assume that the discrepancy of I value between other categories is the smallest and the recognition rate is the best, and then the criterion function can be expressed by the following relation:

$$\min\phi\left(I_{\max}, I_{\min}\right), \quad \phi = I_{\max} - I_{\min}, \tag{9}$$

where $I_{\max}$ and $I_{\min}$ represent the maximum and minimum I values of all categories, respectively.

2.3. Parameter-Optimized ZC Based on Within-Between Distance Models. According to formula (1), we know that the ZC count has nothing to do with the magnitude of signal amplitude and is only related to the positive and negative signs of signals. However, ZC count is sensitive to the presence of noise; as random noises repeatedly cross the coordinate axis in the background, a large number of false ZCR will be generated and affect the recognition result. Equation (1) is suitable for discrete calculation but not conducive to the analysis of related signal waveform. Therefore, formula (1) is firstly transformed into the following equation:

$$C_i = \frac{1}{2}\sum_{n=2}^{N}[1 - \operatorname{sgn}[x(n)\cdot x(n-1)]]. \tag{10}$$

Consider further the influence of random noise; increase a threshold ε to offset part of false ZCR generated by noise repeatedly crossing the coordinate axis. Therefore, the zero-crossing calculation formula can be revised into the form of formula (11):

$$C_i = \frac{1}{2}\sum_{n=2}^{N}[1 - \operatorname{sgn}[x(n)\cdot x(n-1) + \varepsilon]]. \tag{11}$$

The subsequent work is the optimization of threshold ε. The method of extracting ZC features from ZC duration is described in Section 2.1. It is noteworthy that the length of the observation window must greater than the maximum expected time interval between the continuous ZC intervals, so the ZC feature should ensure that the minimum

frequency of interest can be discovered. In order to improve data utilization and maintain data continuity, 50% overlap rate is set. When the maximum expected time is divided into Q intervals by the threshold of $Q+1$, Q group eigenvectors are generated. We know that the extracted features are different on various time scales; therefore, the eigenvector is affected by the length and number of observation window. Literature [36] has discussed the optimization method of these two thresholds, here, the optimized window data are used directly. Keep the optimized window data unchanged, and change the value of ε to extract the ZC feature, respectively. The ε must be changed by the specified step size and adjusted for ZC features changes. Calculate the interclass distance and intraclass distance of each ZC feature. Then, values of I with diverse values of ε are calculated according to formula (9). If the critical point is found, the optimized ε value is obtained. The flow chart of improved method of ZC features extraction is manifested in Figure 1.

Detailed descriptions of the flow chart in Figure 1:

Step 1. Input original vibration signals.

Step 2. Calculate the peak-to-peak value, as the basis for calculating the search step size and search scope.

Step 3. Set the search range and step size of ε. The search step size needs to be based on the experience of making multiple attempts at the actual signal. In the simulation, one-thousandth of the peak value is used as the step length, and 20 steps are used as the search range.

Step 4. Extract ZC feature vectors of every signal at different ε values. The number and length of observation window were optimized before feature extraction, and the data overlapped by 50%.

Step 5. Calculate the value of I between different state categories according to formula (8). Suppose there are 4 kinds of state signals, and then 6 values of I are formed, one for every 2 kinds of signals. ε value is searched 20 times, and then a 6×20 matrix is formed.

Step 6. Calculate the maximum and minimum of I for each search, guaranteed the highest recognition capacity of the two categories is not weakened, and increase the value of I between the two classes that are most difficult to recognize. So, when formula (9) is satisfied, the optimization is achieved. According to the step size of each signal and the number of steps, the optimized ε value of each signal can be obtained.

Step 7. According to the optimized ε value of each signal, extract the optimized ZC features.

Step 8. Bring the optimized features into neural network for fault diagnosis and verification, and the results are analyzed.

3. Simulation Analysis

For the sake of verifying the necessity and effectiveness of the presented method, four simulated signals of normal, inner ring fault, rolling element fault, and outer ring fault of rolling bearing are used for analysis. The simulation signals are obtained from the following formula:

$$\left.\begin{aligned} x(t) &= \sum_{i=1}^{M} A_i s\left(t - iT - \tau_i\right) + n(i) \\ A_i &= A_0 \cos\left(2\pi Q t + \varphi_A\right) + C_A \\ s(t) &= e^{-Bt} \sin\left(2\pi f_n t + \varphi_w\right) \end{aligned}\right\}, \tag{12}$$

where the system sampling frequency $f_s = 12000$ Hz, the resonant frequency $f_n = 3000$ Hz, the inner ring fault frequency $f_i = 162$ Hz, the rolling element fault frequency $f_b = 142$ Hz, the outer ring fault frequency $f_i = 142$ Hz, the rotational frequency $f_r = 30$ Hz, and the damping ratio $B = 400$. Four simulated signals are a group, a total of three groups. Three random noises with a SNR of 30 dB, 5 dB, and −5 dB are added separately to three groups signal. The grouping of simulation signals is shown in Table 1.

3.1. Analysis of ZC Feature Noise Resistance. In order to make the extracted features represent the running state information of the bearing effectively, the length of the data segment calculated with ZC feature should contain at least one complete rotation period. The rotational frequency is 30 Hz, so the length of an observation window must greater than 1/30 seconds which contains 360 points at the sampling frequency of 12 K. Follow the method in Section 2.3 above, the data fragment length is 512, and the number of fragment is 8. As described earlier, the data overlap rate is set to 50%, which contains 256 points at the sampling frequency of 12 K. Each state data are divided into 40 samples and contain data of 0.5 seconds (6000 points). Figure 2 shows the ZC features (FV_{duration}) of the four state signals extracted from each set of signals when SNR = 30, 5, and −5. From the left to the right of the figure is the distribution of FV_{duration} of four state signals when SNR is 30, 5 and −5. The graphs above the figure are the distribution of all samples under a certain feature, and the below ones are the differentiation of all eigenvectors under a certain sample. It can be seen from the three groups of graphs that the ZC feature is very sensitive to random noise, and the recognition ability between ZC features of various state signals is decreasing with random noise increasing. When SNR = 30, FV_{duration} still has fairish recognition ability; however, when SNR = −5, recognition ability of FV_{duration} begins to fail.

3.2. Analysis of ε Value. On the basis of the method description in Section 2.3, extract the ZC features and calculate the various values of I with different values of ε. Then, calculate the values of ϕ according to formula (9) and find the minimum value of ϕ. The relationship between ϕ and ε is shown in Figures 3–5 under different kinds of SNRs. The figures indicate that, with the increase of the ε value, the capacity of distinguish fault is improved, but they will not continue indefinitely. In other words, specifically, value of ϕ would not always decrease but has a critical value, such as the values marked with arrows in three figures, and then with the value of ϕ increasing, the recognition capacity of certain two types will decrease. Therefore, the optimized values of ε can be obtained in a different kind of SNR. The value of ε is represented by the

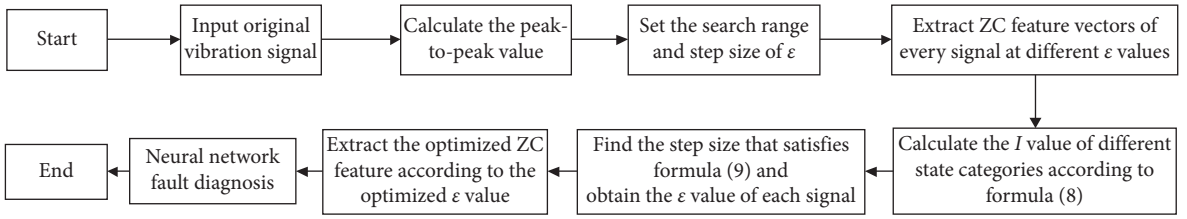

Figure 1: Flow chart of the optimized parameter.

Table 1: The grouping of simulation signals.

Index	SNR = 30	SNR = 5	SNR = −5
Simulated normal\no fault	S11	S21	S31
Simulated inner ring fault	S12	S22	S32
Simulated rolling element fault	S13	S23	S33
Simulated outer ring fault	S14	S24	S34

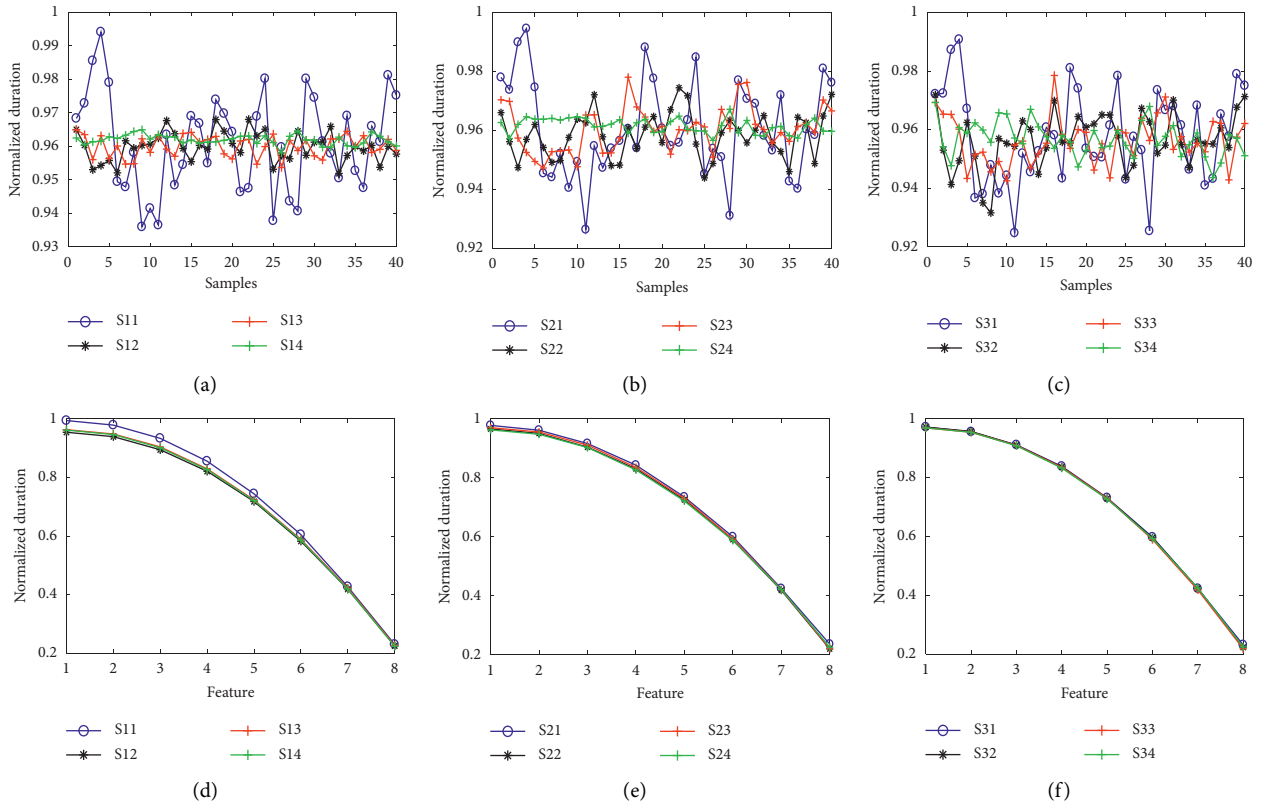

Figure 2: ZC features of four state signals (from left to right, SNR is 30, 5, and −5, respectively).

number of steps, and the step sizes of the four state signals under different kind SNR are shown in Table 2.

It can be seen from Figures 3–5 that the optimal number of steps correspond to the minimum ϕ, combined with the step size in Table 2, and the optimized ε value can be calculated, as shown in Table 3.

Then, the ZC features extracted from above optimized ε values are shown in Figure 6.

From Figure 6, we can clearly see that all samples of signals in diverse states in the same feature can be separated from each other, and similarly, all features of signals in diverse states under the same sample can be separated from each other. Consequently, the ZC characteristics of the four states can be recognized. Compared with the identification result before optimization in Figure 2, the effectiveness of the method is proved.

3.3. Optimization Validation. In order to further prove the availability of the method, the optimized ZC eigenvectors are identified by three-layer feed-forward neural network, and the result of verification is shown in Table 4, which is the

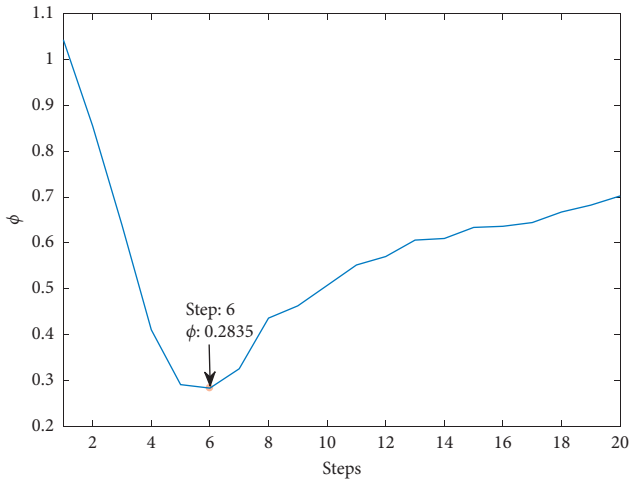

Figure 3: SNR = 30, ϕ and steps trend.

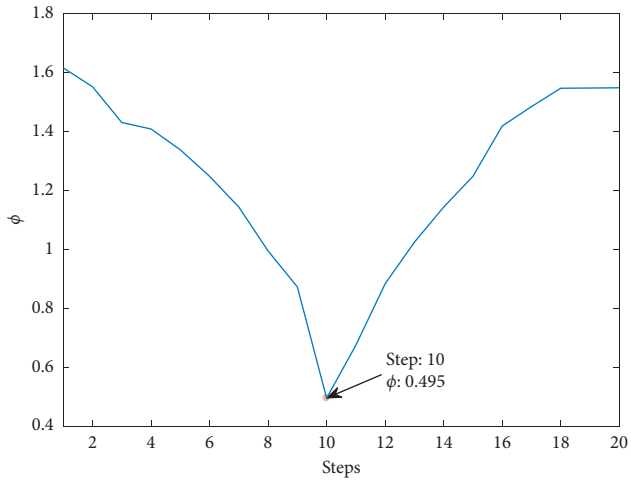

Figure 4: SNR = 5, ϕ and steps trend.

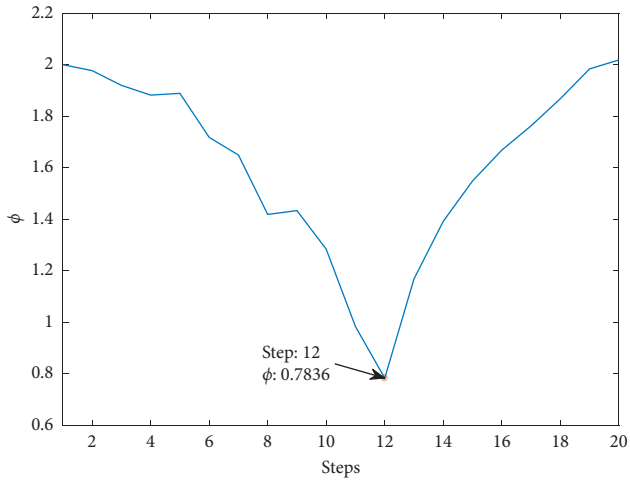

Figure 5: SNR = −5, ϕ and steps trend.

Table 2: The step sizes of the four state signals under different SNRs.

SNR = 30	S11	S12	S13	S14
Step size	0.001	0.008	0.012	0.020
SNR = 5	S21	S22	S23	S34
Step size	0.002	0.007	0.011	0.020
SNR = −5	S31	S32	S33	S34
Step size	0.003	0.009	0.012	0.020

Table 3: The optimized ε value of the four state signals under different SNRs.

SNR = 30	S11	S12	S13	S14
ε	0.006	0.048	0.072	0.12
SNR = 5	S21	S22	S23	S34
ε	0.02	0.07	0.11	0.20
SNR = −5	S31	S32	S33	S34
ε	0.036	0.108	0.144	0.24

average recognition rate of 40 replicates. It can be demonstrated from Table 4 that this method has a high fault identification rate for REB simulation signals.

4. Experiment Validation

The necessity and effectiveness of the improved model and parameter optimization are verified by simulation experiments. In practical applications, the identification of rolling bearing faults usually requires the identification method to be robust for load, so the experiment uses the bearing data from the Case Western Reserve University Bearing Data Center to verify whether the proposed method is effective.

4.1. Experiment Data and Schemes. The bearing status data set is derived from [37]. The type of test bearing is deep groove bearing, and the data are sampled by the accelerometer at 12 KHz from the drive end of the motor. Single-point failure diameter is 0.007 inches. The outer ring failure is located at 6 o'clock. For the motor loads 0, 1, 2, and 3, motor speeds are from 1797 to 1730 RPM. Table 5 details the load and speed.

The whole experiment consists of three parts. The first experiment verifies the identification effect of four bearing states under load 0 HP and compares with the traditional ZC methods. Then, the bearing state data at load 0 are used as the training set to test the fault identification effect of the bearing state data under other loads. Finally, the bearing state data under any load are used as the training set to test the fault identification effect of the bearing state data under other loads. The first part of the experiment is to verify the effect of the method in practical application, and the remaining two parts are used to test the robustness of the method.

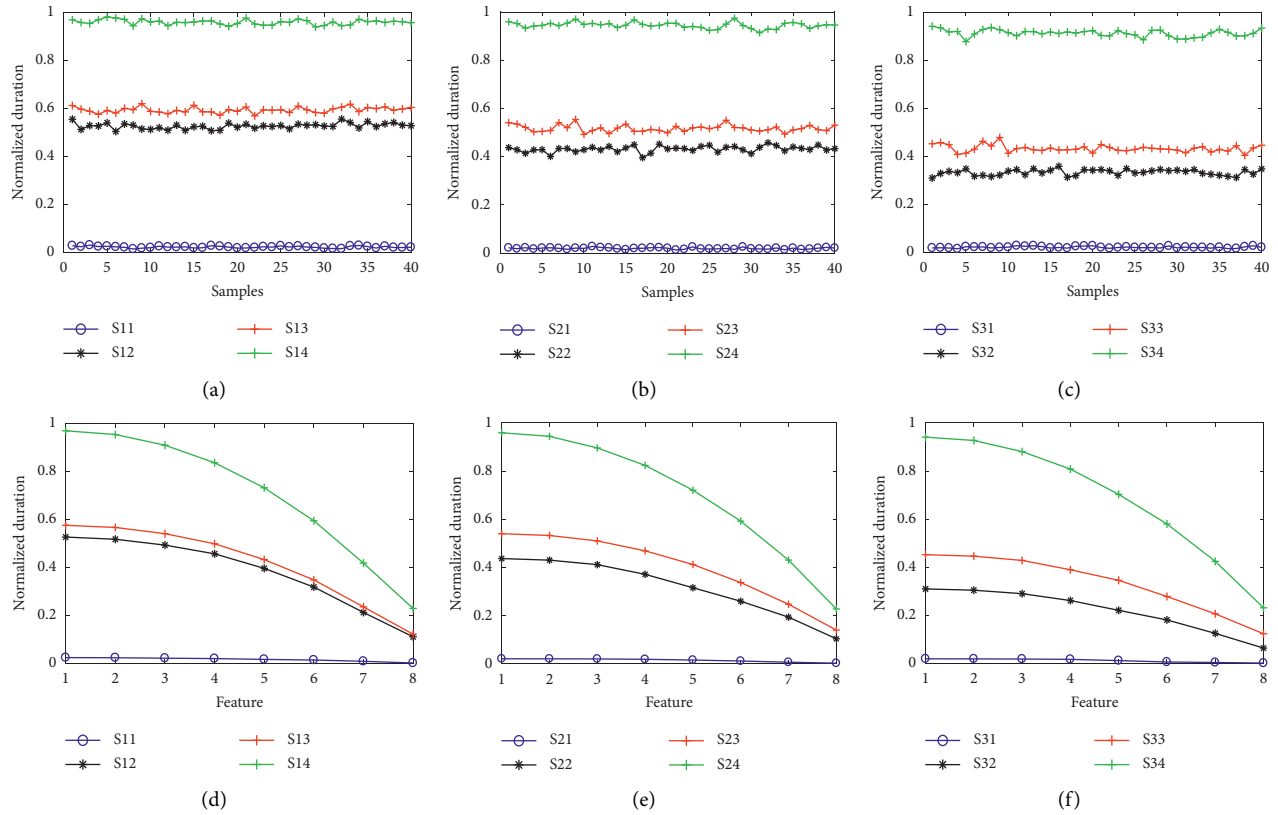

Figure 6: Optimized ZC features of four state signals (from left to right, SNR is 30, 5, and −5, respectively).

Table 4: The average identification rate of simulation fault.

Index	SNR = 30	SNR = 5	SNR = −5
Classification rate (%)	FV_{duration}	FV_{duration}	FV_{duration}
Normal	100	100	100
Inner ring defect	100	100	99.85
Rolling element defect	100	100	99.85
Outer ring defect	100	100	100

Table 5: The motor load and corresponding speed.

Index	Load 0	Load 1	Load 2	Load 3
Motor speed/RPM	1797	1772	1750	1730

4.2. Results and Analysis. Firstly, the spectrum and envelope spectrum analysis of bearing state data under load 0 test are carried out to understand the influence of noise on fault diagnosis. Figures 7 and 8 show the frequency spectrum and envelope spectrum of normal state, inner ring fault, rolling element fault, and outer ring fault of REB. Due to the modulation of the noise signal, the characteristic frequency cannot be detected from the frequency spectrum. In Figure 8, the characteristic frequency of outer ring failure and the frequency doubling can be observed, but the fault characteristic frequency of the inner ring is not obvious and the characteristic frequency of rolling element is unavailable. So, the fault of rolling element cannot be identified effectively as the influence of strong noise and signal modulation, and the random signal is spread throughout the frequency domain. It can be concluded from the above analysis that, in practice, random noise abundant is an important factor hindering the accuracy of fault identification. Due to the existence of high frequency noise, it is necessary to improve the ZC method model and optimize the parameters, so as to improve the accuracy of fault diagnosis and make the advantages of fast calculation of ZC method useful.

The rotational speed of load 0 is 1797 rpm from Table 5; therefore, the magnitude of the observation window should be greater than 0.034 seconds which contains 360 points at the sampling frequency of 12 K. Follow the method in Section 3.1, the data fragment length is 720, and the number of fragment is 8. Then, each length of data collected from the four bearing states is 10 seconds, which is divided into 40 segments with 50% overlap rate. According to the method in this paper, optimization parameters in the improved model, respectively, are calculated and shown in Table 6. The ratio shows the ratio of the optimized ε to the value of peak-to-peak. Figure 9 shows the comparison of ZC characteristics of four bearing states before and after the model improvement and parameter optimization.

From Figures 9(a) and 9(c), we can see that, before the model improvement parameter optimization, the fault characteristics of partial samples of rolling element and outer ring are similar and difficult to distinguish, which will lead to misjudgment. From Figures 9(b) and 9(d), we can see that the sample characteristics of rolling element fault and the outer ring fault are completely distinguished through

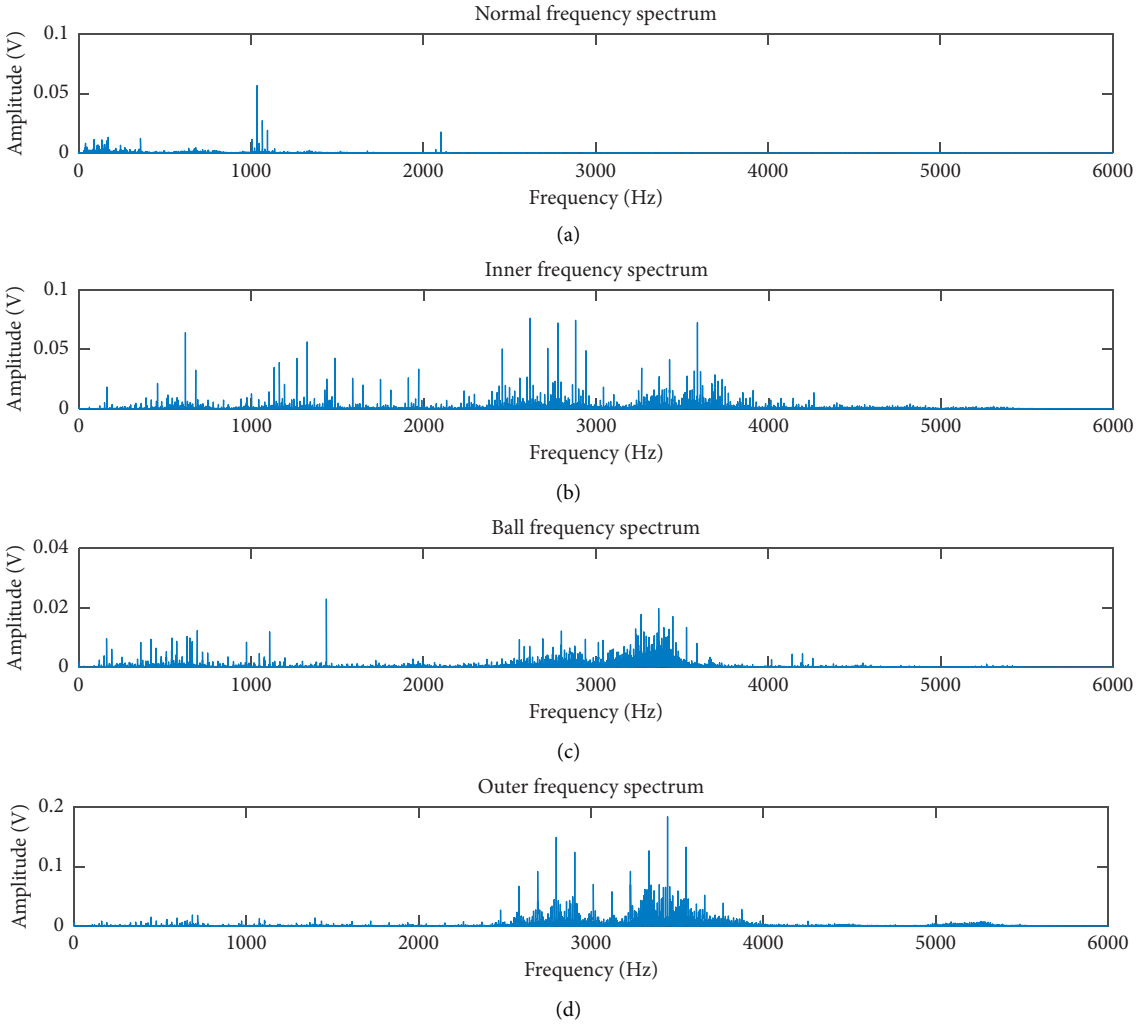

Figure 7: Frequency spectrum of four bearing states.

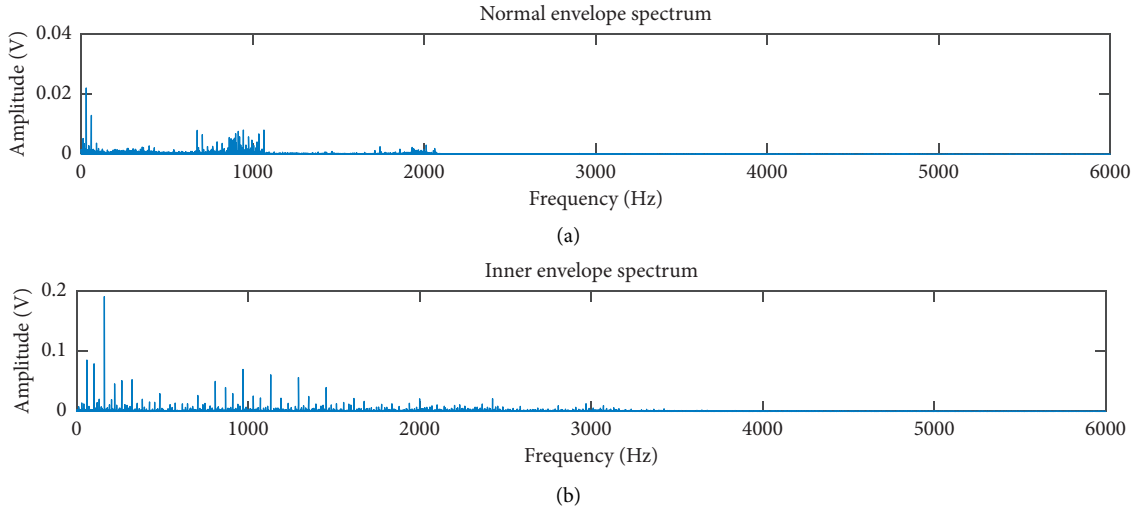

Figure 8: Continued.

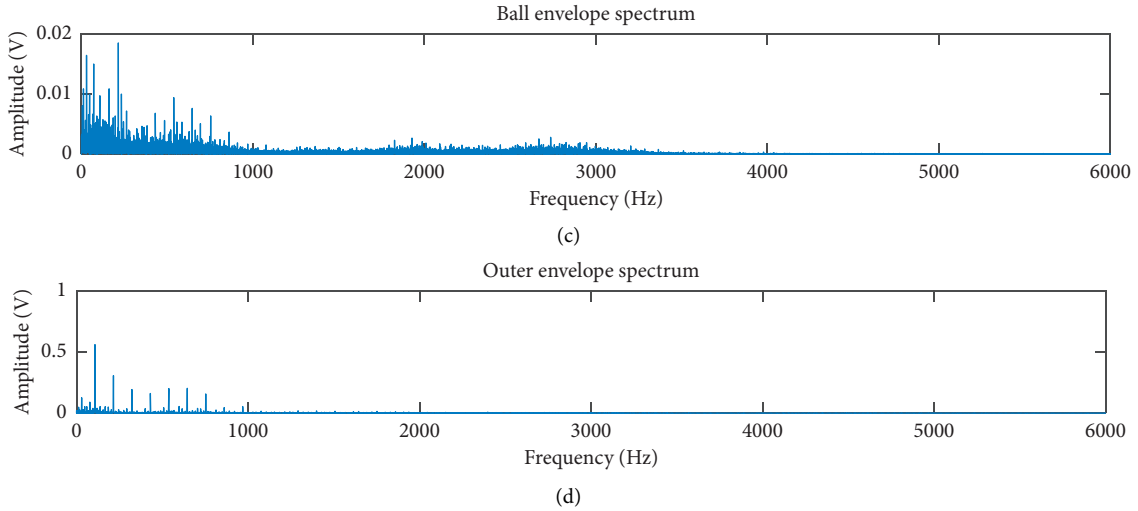

Figure 8: Envelope spectrum of four bearing states.

Table 6: Optimized values of ε and theirs ratios to peak-to-peak.

Index	Normal	Inner race fault	Ball fault	Outer race fault
ε	0.000598	0.003109	0.001211	0.002041
Ratio (%)	0.1	0.1	0.1	0.029

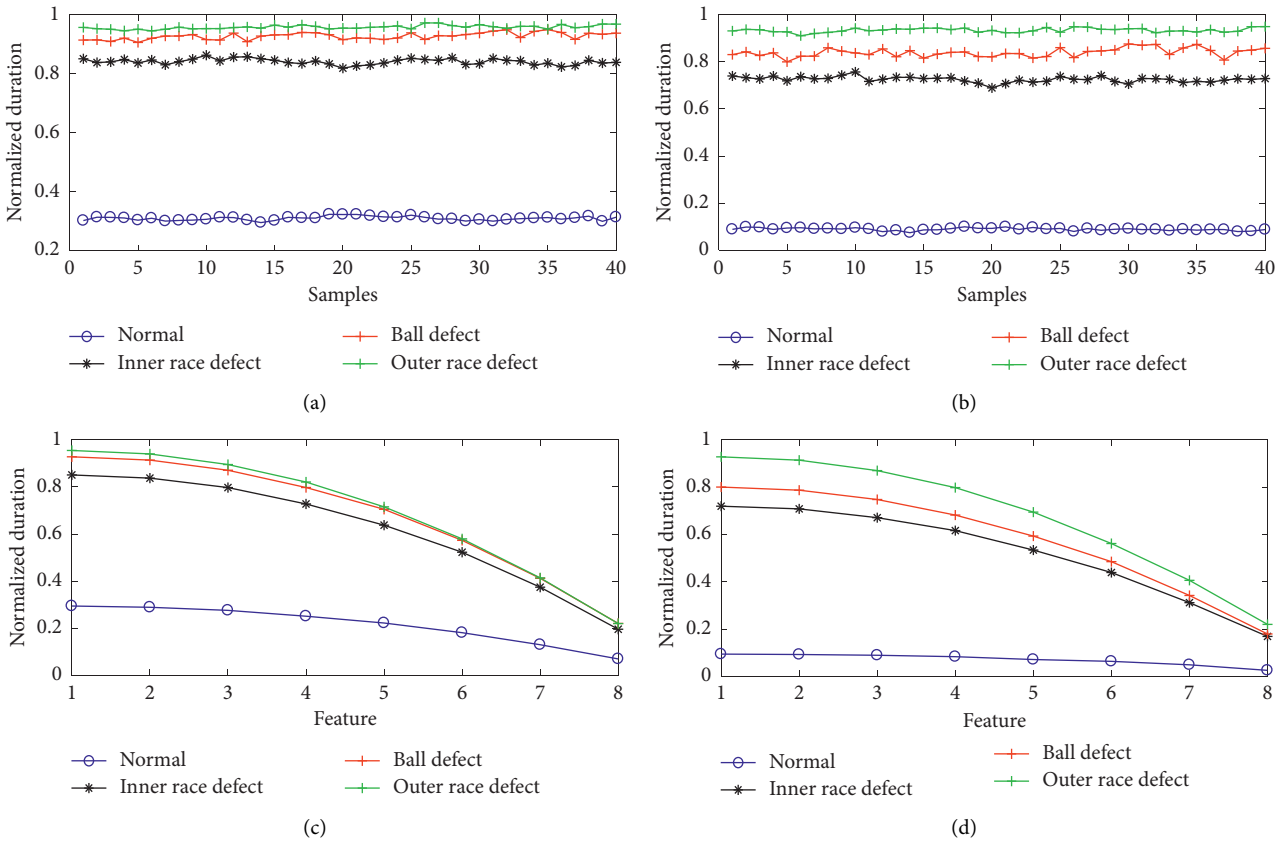

Figure 9: ZC duration features before (a and c) and after (b and d) the model improvement and parameter optimization.

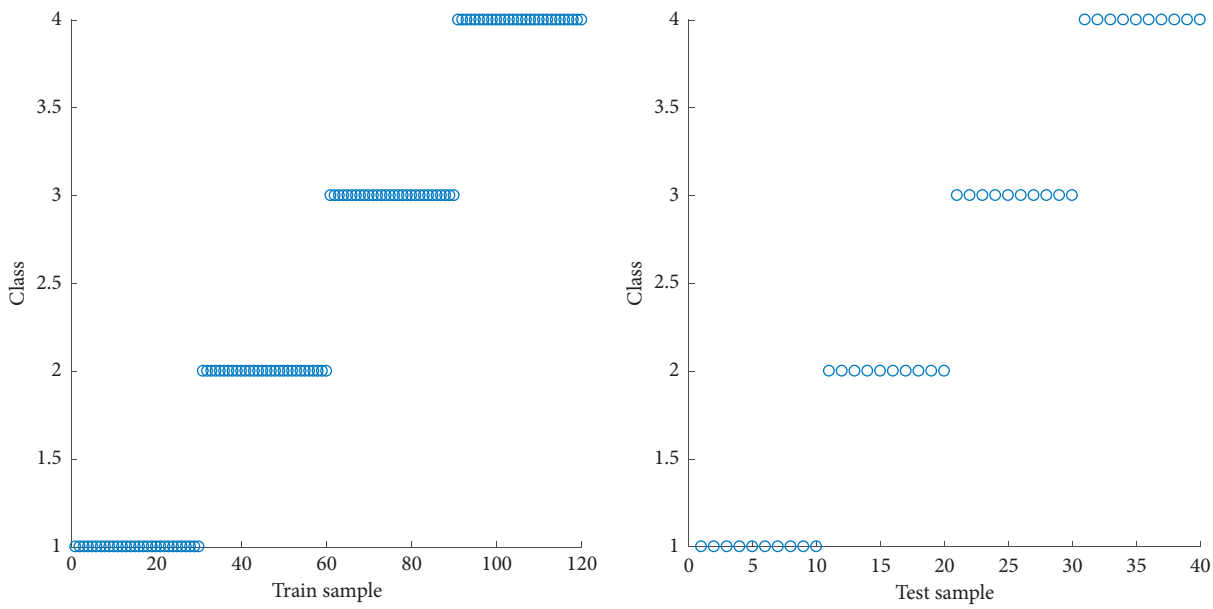

Figure 10: Identification results of adopting the method of the model improvement and parameter optimization.

Table 7: Comparison of mean recognition rate before and after optimization.

Index	Training set	Test set
Accuracy of before optimization (%)	93.33	92.25
Accuracy of after optimization (%)	100	100

Table 8: Optimized ε values of various bearing states under three loads.

Index	Normal	Inner ring fault	Rolling element fault	Outer ring fault
ε under load 1	0.000521	0.002938	0.001299	0.001776
ε under load 2	0.000635	0.003065	0.001171	0.001793
ε under load 3	0.000548	0.003188	0.001321	0.001809

Table 9: Recognition rate of various bearing states under three loads.

Index	Normal	Inner ring fault	Rolling element fault	Outer ring fault
Accuracy of load 1 (%)	100	100	99.17	99.17
Accuracy of load 2 (%)	100	97.5	95	92.5
Accuracy of load 3 (%)	99.17	99.17	98.33	98.33

adopting the method of the model improvement and parameter optimization.

In order to compare the recognition rate, all the eigenvectors are taken to a three-layer neural network, whose weights and thresholds are optimized by genetic algorithm to improve the diagnostic efficiency and accuracy. The number of neurons in the hidden layer is 5, and the total number of samples is 160, including training set sample 120 and test set sample 40. Each bearing state contains 30 training set samples and 10 test set samples, arranged in order according to normal, inner ring fault, rolling element fault, and outer ring fault. The result of verification is shown in Figure 10, which is the average recognition rate of 40 replicates. The recognition rate of both training prior statistics and test set is always 100% and proves that purposed method can identify bearing faults accurately.

Table 10: Recognition rate of different load HPs as training sets.

Index	Test set recognition rate			
Training set	Load 0	Load 1	Load 2	Load 3
Load 0	100	99.72	96.83	99.12
Load 1	98.13	99.85	96.72	97.83
Load 2	97.75	97.28	98.83	97.52
Load 3	98.15	97.23	96.95	99.17

As a comparison, the recognition result before the model improvement and parameter optimization is shown in Figure 11.

The results in the Figure 11 represent the average recognition accuracy of 40 repeated experiments, from which it can be intuitively seen that the recognition rate of normal state and inner ring fault is 100%, but the recognition rate of rolling element fault and outer ring fault is not satisfactory. The partial misjudgment between rolling element fault and outer ring fault has affected the fault recognition rate, and the comparison of the average recognition rate of 40 experiments is shown in Table 7.

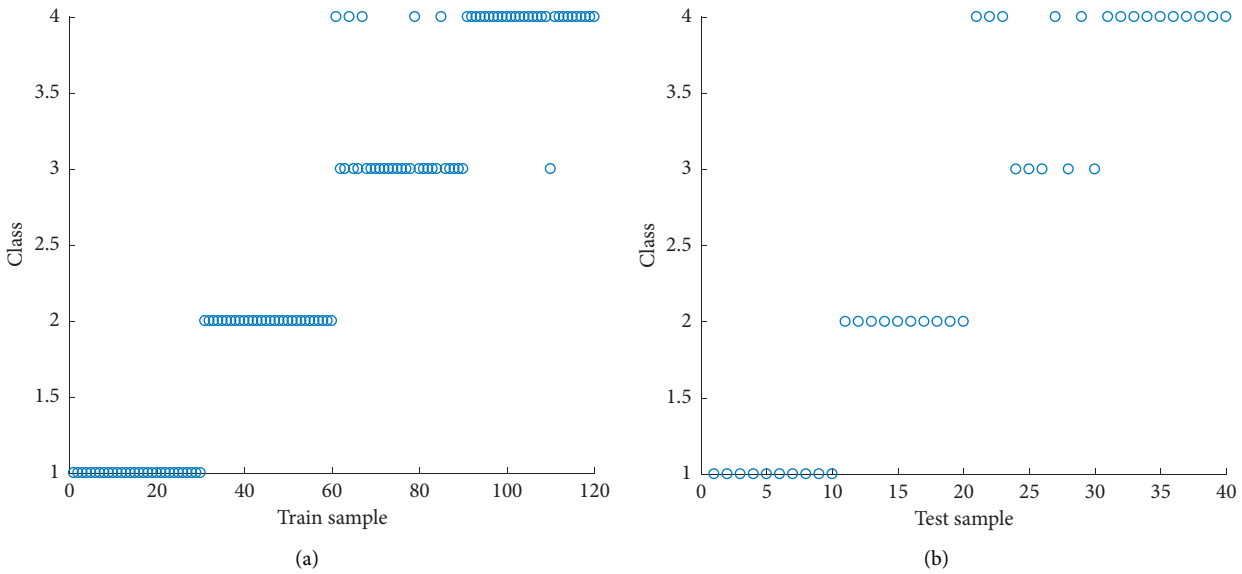

Figure 11: Identification results before the model improvement and parameter optimization.

The experimental results show that the method of the model improvement and parameter optimization is effective for bearing fault identification under the same load.

Next, the experiment will verify whether the method in this paper is robust for the load. The experimental data of load 0 is still used as the training set; according to ratios of ε to peak-to-peak in Table 6, calculate the optimization parameters under the other load and extract the ZC features as the test set. The length and number of observation windows should be consistent with that under load 0 when extracting the ZC features under other load. Table 8 shows the optimized ε values of various bearing states and under three loads.

The same neural network is applied to identify the bearing fault, and the results are shown in Table 9.

According to the recognition results in Table 9, although the fault recognition rate at load 2 is lower, the overall recognition rate of other loads still achieves the expected effect. The analysis of the error identification samples shows that these samples are quite distinct from the other samples of the same state, so the validity of the method is not affected. The experiment proves that the method is applicable to other loads when the load information is known.

Finally, the experiment verifies the test effect under any load, and the recognition effect of unknown load has been tested. Similarly, the method proposed in this paper is employed for obtaining characteristic samples, the samples under each load are used as training sets, and the samples of other load are test sets. The overall recognition rate measured is shown in Table 10, and each result is the average recognition rate of 40 tests as well.

According to the analysis of the results presented in Table 10, the recognition accuracy of samples under the same load as the training set and the test set is relatively high. When samples under different loads are used as training sets to test other load samples, the recognition accuracy is slightly lower because a few samples deviate from the characteristics of similar samples. In general, the experimental results demonstrate that the method has good load robustness, so as to accurately identify the bearing fault even if the bearing load is not known.

5. Conclusion

In this paper, an improved fault diagnosis method for electromechanical system based on ZC algorithm is proposed, which optimized the calculation model of ZCR and the parameters of ZC algorithm by establishing a criterion function model. The fault diagnosis experiment of motor REB proves that the method successfully overcomes the shortcoming of ZC feature sensitive to noise and can realize accurate fault diagnosis without knowing the bearing load. Combined with the merits of saving computing time, in the case of big data, the method is expected to monitor the crucial parts of electromechanical system in real time, so as to provide security and reliability guaranty for accurate control of the electromechanical system.

Data Availability

The data used to support the study are available from the corresponding author upon request.

Conflicts of Interest

The authors declare that there are no conflicts of interest regarding the publication of this paper.

Acknowledgments

This work was supported by the National Key Research and Development plan of China under Grant 2018YFB1306103, the National Natural Science Foundation of China under Grant 51875272, and the Provincial School Education

Cooperation Project of Yunnan Province under Grant KKDA202001003.

References

[1] M. R. Khoshdarregi, S. Tappe, and Y. Altintas, "Integrated five-Axis trajectory shaping and contour error compensation for high-speed CNC machine tools," *IEEE/ASME Transactions on Mechatronics*, vol. 19, no. 6, pp. 1859–1871, 2014.

[2] R. Colombo, I. Cusmano, I. Sterpi, A. Mazzone, C. Delconte, and F. Pisano, "Test-retest reliability of robotic assessment measures for the evaluation of upper limb recovery," *IEEE Transactions on Neural Systems and Rehabilitation Engineering*, vol. 22, no. 5, pp. 1020–1029, 2014.

[3] B. Xu, D. Wang, Y. Zhang, and Z. Shi, "DOB-based neural control of flexible hypersonic flight vehicle considering wind effects," *IEEE Transactions on Industrial Electronics*, vol. 64, no. 11, pp. 8676–8685, 2017.

[4] X. Ding, Q. He, and N. Luo, "A fusion feature and its improvement based on locality preserving projections for rolling element bearing fault classification," *Journal of Sound and Vibration*, vol. 335, pp. 367–383, 2015.

[5] Y. Zhang and R. B. Randall, "Rolling element bearing fault diagnosis based on the combination of genetic algorithms and fast kurtogram," *Mechanical Systems and Signal Processing*, vol. 23, no. 5, pp. 1509–1517, 2009.

[6] J. Benali, M. Sayadi, F. Fnaiech, B. Morello, and N. Zerhouni, "Importance of the fourth and fifth intrinsic mode functions for bearing fault diagnosis," in *Proceedings of the 14th International Conference on Sciences and Techniques of Automatic Control & Computer Engineering—STA'2013*, Sousse, Tunisia, December 2013.

[7] S. Nandi, H. A. Toliyat, and X. Li, "Condition monitoring and fault diagnosis of electrical motors-A review," *IEEE Transactions on Energy Conversion*, vol. 20, no. 4, pp. 719–729, 2005.

[8] J. Huang, S. Ri, T. Fukuda, and Y. Wang, "A disturbance observer based sliding mode control for a class of underactuated robotic system with mismatched uncertainties," *IEEE Transactions on Automatic Control*, vol. 64, no. 6, pp. 2480–2487, 2019.

[9] J. Huang, M. Zhang, S. Ri, C. Xiong, Z. Li, and Y. Kang, "High-order disturbance observer based sliding mode control for mobile wheeled inverted pendulum systems," *IEEE Transactions on Industrial Electronics*, vol. 67, no. 3, pp. 2030–2041, 2020.

[10] H. Jian, M. H. Ri, D. Wu, and S. Ri, "Interval type-2 fuzzy logic modeling and control of a mobile two-wheeled inverted pendulum," *IEEE Transactions on Fuzzy Systems*, vol. 26, no. 4, pp. 2030–2038, 2018.

[11] P. D. Mcfadden and J. D. Smith, "Model for the vibration produced by a single point defect in a rolling element bearing," *Journal of Sound and Vibration*, vol. 96, no. 1, pp. 69–82, 1984.

[12] N. Sawalhi and R. B. Randall, "Simulating gear and bearing interactions in the presence of faults," *Mechanical Systems and Signal Processing*, vol. 22, no. 8, pp. 1924–1951, 2008.

[13] Q. Zhu, L. Liu, S. Li, and W. Zhang, "Control of complex nonlinear dynamic rational systems," *Complexity*, vol. 2018, Article ID 8953035, 12 pages, 2018.

[14] Q. M. Zhu, D. Y. Zhao, and J. Zhang, "A general U-block model-based design procedure for nonlinear polynomial control systems," *International Journal of Systems Science*, vol. 47, no. 14, pp. 3465–3475, 2015.

[15] A. Rafsanjani, S. Abbasion, A. Farshidianfar, and H. Moeenfard, "Nonlinear dynamic modeling of surface defects in rolling element bearing systems," *Journal of Sound & Vibration*, vol. 319, no. 3-5, pp. 1150–1174, 2009.

[16] T. W. Rauber, F. de Assis Boldt, and F. M. Varejao, "Heterogeneous feature models and feature selection applied to bearing fault diagnosis," *IEEE Transactions on Industrial Electronics*, vol. 62, no. 1, pp. 637–646, 2015.

[17] J. Chebil, M. Hrairi, and N. Abushikhah, "Signal analysis of vibration measurements for condition monitoring of bearings," *Australian Journal of Basic & Applied Sciences*, vol. 5, no. 1, p. 70, 2011.

[18] M. D. Prieto, G. Cirrincione, A. G. Espinosa, J. A. Ortega, and H. Henao, "bearing fault detection by a novel condition-monitoring scheme based on statistical-time features and neural networks," *IEEE Transactions on Industrial Electronics*, vol. 60, no. 8, pp. 3398–3407, 2013.

[19] A. Garcia-Perez, R. d. J. Romero-Troncoso, E. Cabal-Yepez, and R. A. Osornio-Rios, "The application of high-resolution spectral analysis for identifying multiple combined faults in induction motors," *IEEE Transactions on Industrial Electronics*, vol. 58, no. 5, pp. 2002–2010, 2011.

[20] Z. K. Peng and F. L. Chu, "Application of the wavelet transform in machine condition monitoring and fault diagnostics: a review with bibliography," *Mechanical Systems and Signal Processing*, vol. 18, no. 2, pp. 199–221, 2004.

[21] J. Seshadrinath, B. Singh, and B. K. Panigrahi, "Investigation of vibration signatures for multiple fault diagnosis in variable frequency drives using complex wavelets," *IEEE Transactions on Power Electronics*, vol. 29, no. 2, pp. 936–945, 2014.

[22] W. Su, F. Wang, H. Zhu, Z. Zhang, and Z. Guo, "Rolling element bearing faults diagnosis based on optimal Morlet wavelet filter and autocorrelation enhancement," *Mechanical Systems and Signal Processing*, vol. 24, no. 5, pp. 1458–1472, 2010.

[23] X. Jin, M. Zhao, T. W. S. Chow, and M. Pecht, "Motor bearing fault diagnosis using trace ratio linear discriminant analysis," *IEEE Transactions on Industrial Electronics*, vol. 61, no. 5, pp. 2441–2451, 2014.

[24] M. Zhao, X. Jin, Z. Zhang, and B. Li, "Fault diagnosis of rolling element bearings via discriminative subspace learning: visualization and classification," *Expert Systems with Applications*, vol. 41, no. 7, pp. 3391–3401, 2014.

[25] R. Niederjohn, "A mathematical formulation and comparison of zero-crossing analysis techniques which have been applied to automatioc speech recognition," *IEEE Transactions on Acoustics, Speech, and Signal Processing*, vol. 23, no. 4, pp. 373–380, 1975.

[26] P. William and M. Hoffman, "Efficient sensor network vehicle classification using peak harmonics of acoustic emissions," in *Proceedings of the SPIE Defense and Security Symposium %*, Orlando, FL, USA, March 2008.

[27] A. Shahidi Zandi, R. Tafreshi, M. Javidan, and G. A. Dumont, "Predicting epileptic seizures in scalp EEG based on a variational bayesian Gaussian mixture model of zero-crossing intervals," *IEEE Transactions on Biomedical Engineering*, vol. 60, no. 5, pp. 1401–1413, 2013.

[28] C.-H. Wu, H.-C. Chang, P.-L. Lee et al., "Frequency recognition in an SSVEP-based brain computer interface using empirical mode decomposition and refined generalized zero-crossing," *Journal of Neuroscience Methods*, vol. 196, no. 1, pp. 170–181, 2011.

[29] P. E. William and M. W. Hoffman, "Identification of bearing faults using time domain zero-crossings," *Mechanical Systems and Signal Processing*, vol. 25, no. 8, pp. 3078–3088, 2011.
[30] T. Liu, J. Chen, and G. Dong, "Zero crossing and coupled hidden Markov model for a rolling bearing performance degradation assessment," *Journal of Vibration and Control*, vol. 20, no. 16, pp. 2487–2500, 2013.
[31] A. Ukil, S. Chen, and A. Andenna, "Detection of stator short circuit faults in three-phase induction motors using motor current zero crossing instants," *Electric Power Systems Research*, vol. 81, no. 4, pp. 1036–1044, 2011.
[32] J. D. T. Gonzalez and W. Kinsner, "Zero-crossing analysis of Lévy walks for real-time feature extraction," in *Proceedings of the IEEE International Conference on Electro Information Technology EIT*, Grand Forks, ND, USA, May 2016.
[33] R. G. Waghmare, S. L. Nalbalwar, and A. Das, "Transient signal detection on the basis of energy and zero crossing detectors," *Procedia Engineering*, vol. 30, pp. 129–134, 2012.
[34] B. R. Nayana and P. Geethanjali, "Analysis of statistical time-domain features effectiveness in identification of bearing faults from vibration signal," *IEEE Sensors Journal*, vol. 17, no. 17, pp. 5618–5625, 2017.
[35] C. Fisher, *Encyclopedia of Biometrics*, p. 549, Springer US, Boston, MA, USA, 2009.
[36] Q. Chen, W. Xing, L. Tao, and L. Hua, "Zero-crossing feature extraction based on threshold optimization for rolling element bearing," in *Lecture Notes in Electrical Engineering*, pp. 409–425, Springer, Berlin, Germany, 2018.
[37] Case Western Reserve University Bearing Data Center Website accessed on Mar. 23, 2015. [Online].Available: http://csegroups.case.edu/bearingdatacenter/pages/download-data-file/.